Part I

Solidification Theory and Experiments

A CALORIMETRIC EVALUATION OF THE ROLE OF IMPURITIES IN THE NUCLEATION OF SECONDARY PHASES IN 1xxx Al ALLOYS

C. M. ALLEN*, K. A. Q. O'REILLY*, P. V. EVANS** AND B. CANTOR*
*Oxford Centre for Advanced Materials and Composites, Department of Materials, University of Oxford, Parks Road, Oxford OX1 3PH, U.K.
**Alcan International Limited, Banbury Laboratory, Southam Road, Banbury, Oxon. OX16 7SP, U.K.

ABSTRACT

Superpurity (>99.995wt% pure) 1xxx series Al-0.3wt%Fe-0.1wt%Si alloys with different impurity additions have been melt spun to produce ribbons with microstructures of fine scale ~0.1-0.2μm diameter secondary phase particles entrained in a higher melting point Al matrix. The melting and resolidification behaviour at 2Kmin^{-1} of the secondary phase particles while entrained in the solid matrix was monitored using differential scanning calorimetry, to simulate the nucleation of secondary phases in liquid interdendritic regions during the final stages of solidification in casting. The melting and resolidification behaviour of 500ppm V and Zr doped superpurity ribbons is the same as that of a commercial purity ribbon. This indicates that V is responsible for the promotion of the metastable $FeAl_m$ phase in the commercial purity ribbon. The presence of $FeAl_m$ in direct chill (DC) cast commercial purity alloys indicates that V also influences phase selection in the faster cooled (~5-10Ks^{-1}) regions of these alloys.

INTRODUCTION

Wrought Al alloys are used in a variety of commercially important applications, including packaging, beverage cans, extrusions and automotive components. The secondary phases in these alloys, although often present at <5vol%, have a large effect on material properties including strength, toughness, anodising response, formability and recrystallisation.

Most wrought alloys are *direct chill* (DC) cast [1,2,3] to produce ingots which are subsequently formed. Variations in both solidification velocity and cooling rate across the cross section of the ingot during casting can alter the secondary phase content, size and morphology, by changing the growth and nucleation mechanisms that predominate locally [4]. The variations in phase content are minimised by scalping and homogenisation after casting.

There has been considerable study of the growth behaviour of these secondary phases, using directional solidification techniques such as Bridgman growth [5,6] or electron beam surface remelting [7]. To date however, the mechanisms by which these phases nucleate *prior* to growth have not been systematically investigated. A modified entrained droplet method [8] combined with differential scanning calorimetry (DSC) has been used to study impurity catalysed nucleation of secondary phases in 1xxx Al alloys [9]. Melt spinning produces a fine scale dispersion of low melting point secondary phases in a higher melting point Al matrix, which are then melted to form entrained liquid droplets in the solid matrix. As the liquid droplets are dispersed throughout the matrix each individual droplet requires its own nucleant for solidification, and hence impurities can exert a strong influence. The subsequent resolidification of the droplets is studied using DSC,

Mat. Res. Soc. Symp. Proc. Vol. 481 © 1998 Materials Research Society

to simulate the solidification of the final 10-15% of liquid between the primary Al dendrite arms during DC casting.

EXPERIMENTAL

One Al-0.3wt%Fe-0.1wt%Si alloy, of >99.995wt% pure Al, Fe and Si, and ten Al-0.3wt%Fe-0.1wt%Si-X alloys, of >99.995wt% pure Al, Fe and Si (with X=500ppm Cu, Cr, Mg, Mn, Ti, V, Zn or Zr, 250ppm Ni or 25ppm P) were cast into steel moulds. Compositions as determined by spark emission spectrographic analysis, stated as the mean of three analyses, are listed in Table I. 5g samples of each alloy were rapidly remelted in a quartz crucible under Ar at 4.5×10^4Pa and melt-spun by ejection through a 1mm nozzle using an Ar overpressure of 3.5×10^4Pa onto a Cu wheel rotating at $23 ms^{-1}$. For comparison a commercial purity (>99.95wt% pure) DC cast Al-0.3wt%Fe-0.1wt%Si alloy, of total impurity content <500ppm, including typically <100ppm each of Zn, Ga, V and Ni, was also melt spun. The resulting ribbons were typically 0.1-1m long, <10mm wide and 50-150μm thick. 2mg specimens of these ribbons were sealed into W lined Cu pans and analysed in a TA Instruments 2010 DSC, using an identically prepared empty pan as a reference. Two cycles of partial melting-resolidification DSC, to melt and resolidify the secondary particles only, were performed under a dynamic Ar atmosphere, by heating from 632-658°C at $2 K min^{-1}$, resolidifying at $2 K min^{-1}$ to 632°C, then remelting and resolidifying once more in an identical manner.

alloy	deliberate additions (ppm)	impurities (ppm)
DC4	1:1000 Al-Ti-B grain refiner	<500ppm total, inc. V, Zn, Ga, Ni
CAL	-----	2 Cu, 4 Mn, 3 Mg
CALCu500	500 Cu	7 Mn, 6 Mg, 4Li
CALCr500	560 Cr	2 Cu, 6 Mn, 3 Mg
CALMg500	586 Mg	2 Cu, 4 Mn, 4P
CALMn500	470 Mn	3 Cu, 3 Mg
CALNi250	260 Ni	3 Cu, 5 Mn, 2 Mg, 3P
CALP25	23 P	2 Cu, 13Mn, 2 Mg
CALTi500	460 Ti	2 Cu, 5 Mn, 2 Mg, 4 Ga
CALV500	560 V	2 Cu, 5 Mn, 2 Mg
CALZn500	613 Zn	2 Cu, 5 Mn, 3 Mg
CALZr500	430 Zr	2 Cu, 5 Mn, 3 Mg, 23Ni, 3P

Table I. Impurity contents. All alloys contained 0.30±0.03wt%Fe and 0.10±0.02wt%Si. Elements detected at or below their detection limits (typically 1ppm) : Bi, Pb, Sn, Be, Ca, Cd, Co, Na, Sr.

RESULTS

Table II lists the melting and solidification peak and onset temperatures from the partial melting and resolidification of the melt-spun ribbons of compositions as listed in Table I.

Figs. 1a and 1b show the first cycle partial melting DSC endotherms from the melt-spun ribbons of compositions as listed in Table I. All the endotherms consisted of a doublet. The melting onset temperatures were in the range 650.7±0.8°C (quoted as mean±2 standard deviations), except for that of CALNi250 which was lower at 649.2°C.
Figs. 2a and 2b show the first cycle resolidification DSC exotherms after partial melting. All exotherms contained a large peak with solidification onset temperatures of 652.6±0.6°C, with a range of smaller peaks at lower temperatures labelled A-N. The estimated solidification onset temperatures of these peaks are listed in Table III.
Figs. 3a and 3b show the second cycle partial melting DSC endotherms after partial melting and resolidification. All the endotherms had a large single peak with melting onset temperatures of 650.8±1.0°C, in the same position as the doublet detected in the first melting endotherms from all the ribbons. The endotherms from the commercial purity ribbon and the >99.995wt% pure ribbons containing 500ppm V or 500ppm Zr additions also contained a smaller single peak at a melting onset temperature of 649.2±0.9°C. This peak was absent in the endotherms from all the other ribbons.
The forms of the second cycle resolidification DSC exotherms were the same as for the first cycle resolidification exotherms. All exotherms contained a large peak with solidification onset temperatures of 652.9±0.6°C, in the same position as the large peak detected in the first cycle resolidification exotherms, with again a range of smaller peaks at lower temperatures. The estimated solidification onset temperatures of these peaks are listed in Table III.

DISCUSSION

The double peak present in the endotherms from all alloys on first melting with an onset temperature of 650.7±0.8°C corresponds to the melting of the entrained secondary phases. Two distinct morphologies of the equilibrium Al-Fe_4Al_{13} eutectic result from microstructural equilibration of these alloys during DSC heating [9,10,11]: (i) as-melt spun phases transform to Fe_4Al_{13}; and (ii) excess Fe in solid solution precipitates as Fe_4Al_{13} during heating in the DSC prior to the onset of melting. On first cycle resolidification the solidification of Al-Fe_4Al_{13} is detected as the *single* peak common to all exotherms, with a solidification onset temperature of 652.6±0.6°C and on remelting as the single peak with the same melting onset temperature as the doublet on first melting, namely 650.8±1.0°C. On second cycle resolidification the solidification of Al-Fe_4Al_{13} is again detected as the single peak common to all exotherms, with a solidification onset temperature of 652.9±0.6°C. The presence of Al-Fe_4Al_{13} has been confirmed by EDX and SADP analysis of particles extracted from the matrix [12]. Figs. 4a, b and c show the bright field TEM micrograph, selected area diffraction pattern and indexed schematic of that pattern from a Fe_4Al_{13} particle extracted from the CAL ribbon after partial melting and resolidification.

In the commercial purity ribbon there are two additional resolidification peaks labelled A and B, with solidification onsets of 647.3°C and 642.6°C respectively. Peak A has been previously shown by isothermal holding experiments [10] to correspond to the solidification of a metastable phase. Solidification and subsequent remelting of this phase is not detected in the

alloy	$T_{1m,o}$ /°C	Peaks /°C	$T_{1s,o}$ /°C	Peaks /°C	$T_{2m,o}$ /°C	Peaks /°C	$T_{2s,o}$ /°C	Peaks /°C
DC4	650.9	653.8 655.2	652.8	651.6 645.3 642.0	649.2	651.5 655.0	653.2	651.7 645.3 642.2
CAL	650.0	653.4 654.8	652.8	651.4 639.5	651.2	654.5	653.2	651.6 640.0
Cu500	649.9	652.9 654.4	652.4	651.5	650.6	654.3	652.8	651.1 638.8
Cr500	650.5	653.0 654.7	652.4	651.0 ????	650.7	654.3	652.6	651.3 639.2
Mg500	650.3	653.0 654.4	652.5	650.9 639.4?	651.0	654.7	652.6	651.2 ????
Mn500	651.0	653.6 654.9	652.6	651.0 641.3	651.2	654.5	653.0	651.3
Ni250	649.2	653.0 654.3	652.5	651.0 639.4	649.9	654.4	652.9	651.3 639.2
P25	650.7	653.3 654.9	652.8	651.3 642.3	651.0	654.4	652.8	651.3 642.5
Ti500	650.5	652.7 654.5	652.0	650.4 640.6	650.5	654.2	652.4	651.2 640.8
	651.3	653.5 655.3	652.8	651.2 642.7	651.4	655.2	653.3	652.0 642.9
V500	651.0	653.5 655.3	652.9	651.4 644.7	649.4	651.4 655.1	653.1	651.6 644.8
	650.7	653.9 655.7	652.6	651.4 644.8	649.5	651.3 655.3	652.7	651.4 644.8
Zn500	651.0	652.4 654.1	653.0	650.7 639.7	651.3	652.9	653.2	651.1 640.2
	650.3	652.9 654.6	653.0	652.1 ????	650.2	654.1	653.4	652.4 ????
Zr500	650.3	653.0 654.3	652.2	651.3 639.5	648.5	650.3 654.4	652.5	651.2 639.6

Table II. Melting and solidification onset and peak temperatures (where determined)

Note: $T_{1m,o}$ and $T_{2m,o}$ denote melting onsets on first and second partial melting respectively
$T_{1s,o}$ and $T_{2s,o}$ denote solidification onsets on resolidification after one and two cycles of partial melting respectively

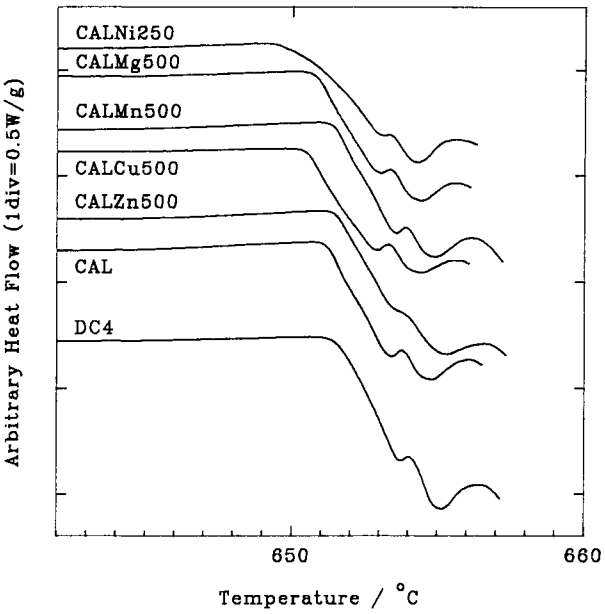

Fig. 1a. Partial melting endotherms

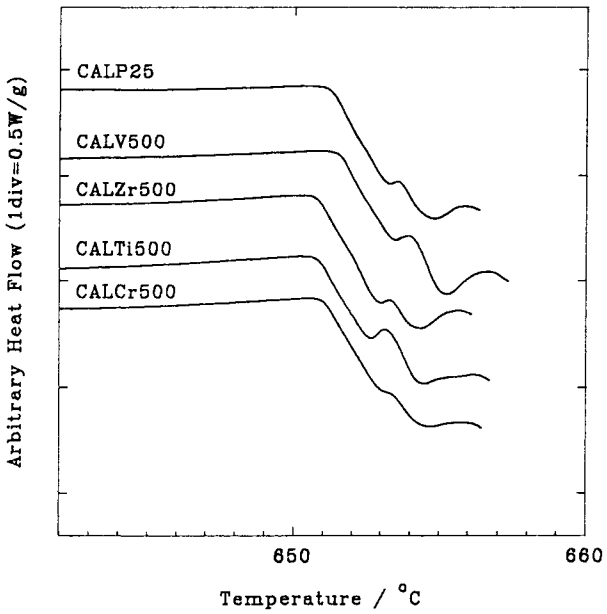

Fig. 1b. Partial melting endotherms

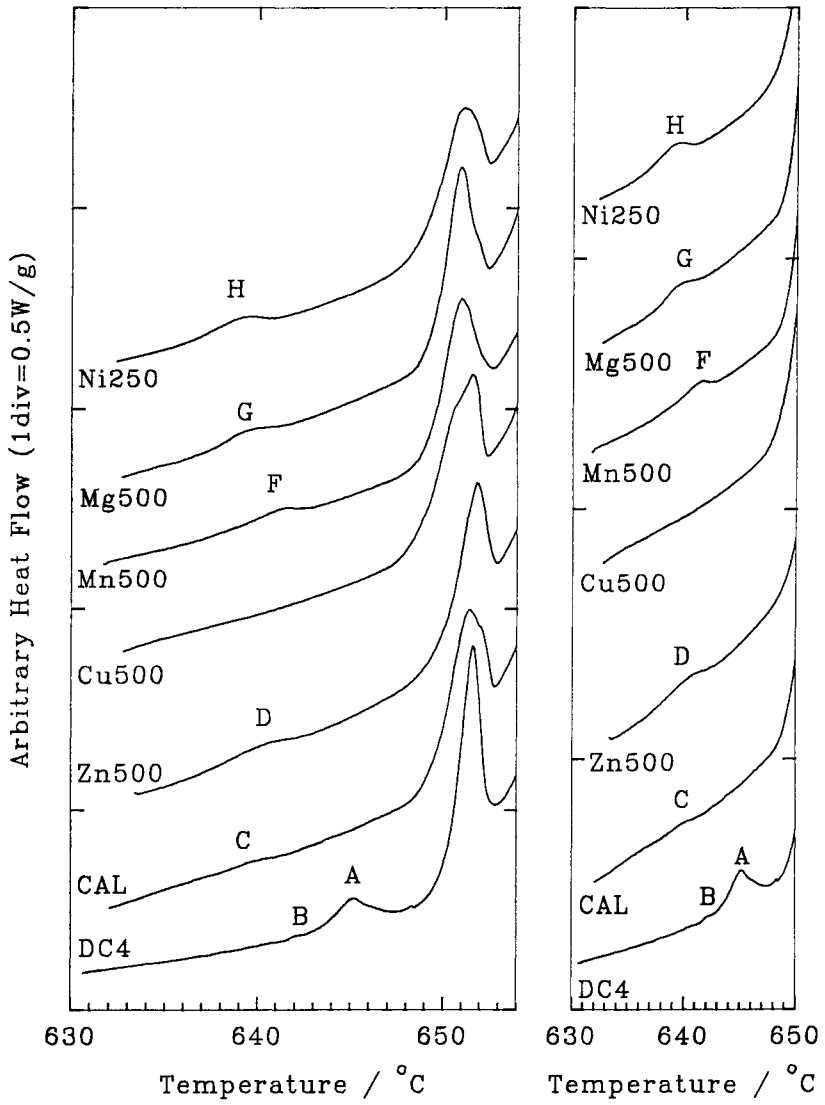

Fig. 2a. Resolidification exotherms (same data plotted on two scales)

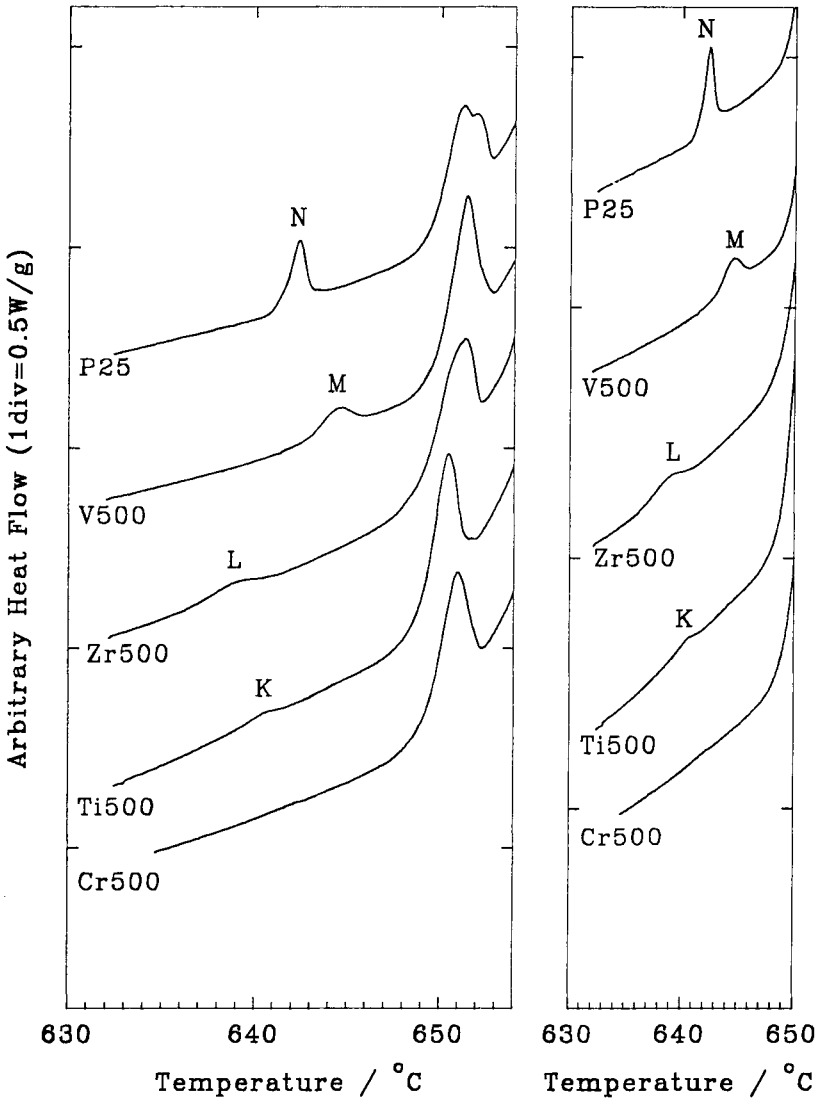

Fig. 2b. Resolidification exotherms (same data plotted on two scales)

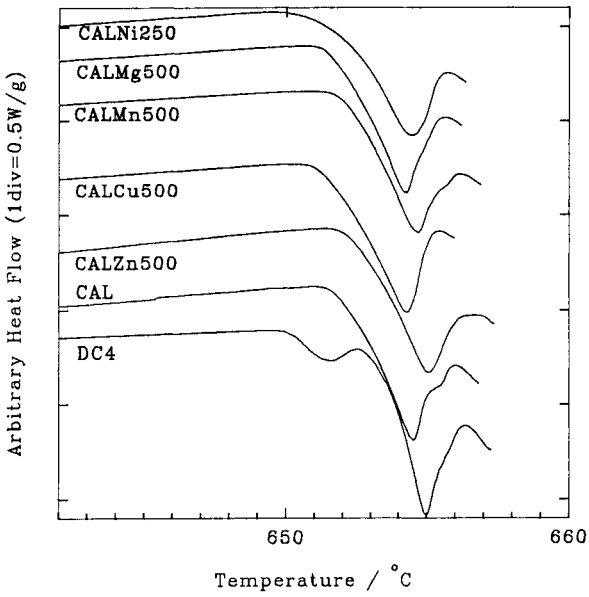

Fig. 3a. Remelting endotherms after partial melting and resolidification

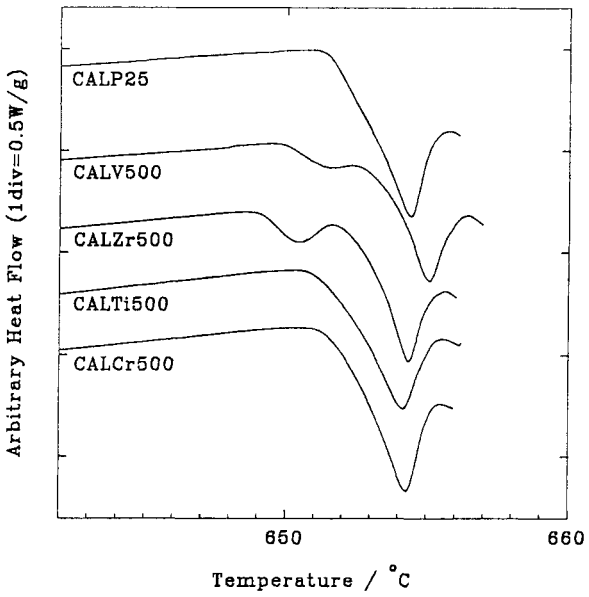

Fig. 3b. Remelting endotherms after partial melting and resolidification